ACS Energy LETTERS

http://pubs.acs.org/journal/aelccp

LETTER

Nanostructured Bulk-Heterojunction Solar Cells Based on Amorphous Carbon

Francesca Risplendi,[†] Giancarlo Cicero,[‡] and Jeffrey C. Grossman*[,†]

[†]Department of Materials Science and Engineering, Massachusetts Institute of Technology, Cambridge, Massachusetts 02139, United States

[‡]Department of Applied Science and Technology, Politecnico di Torino, C.so Duca degli Abruzzi 24, 10129 Torino, Italy

Supporting Information

ABSTRACT: Amorphous carbon (a-C) has the potential to provide properties important to solar photovoltaics that are comparable to those of silicon-based materials with further advantages such as low cost, solution processing, air stability, and higher thermal resistance. We employ accurate computational approaches to explore and understand active layers based on bulk heterojunctions containing a-C. Our results show that interfaces with a-C and other carbon nanostructures could enable successful electron and hole extraction as well as reduced sources for carrier recombination. Ab initio molecular dynamics and density functional theory calculations are carried out for a large statistical set of interfaces between a-C structures of different densities and either carbon nanotubes or fullerenes. We show that the energy alignment at such interfaces can be widely tuned as a function of a-C density, doping chemistry, or nanostructure size to obtain type-II heterostructures and that the optical properties of such interfaces would be highly favorable for sunlight harvesting.

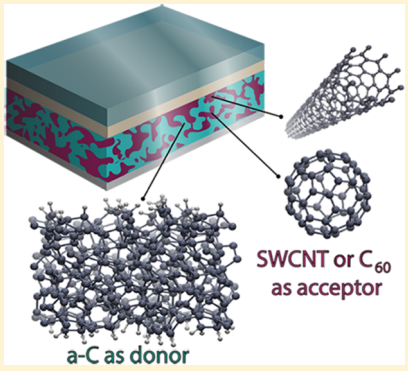

Among the many active layer materials used in thin-film photovoltaic (PV) devices, combinations of carbon nanomaterials such as graphene, carbon nanotubes (CNTs), fullerenes, and amorphous carbon (a-C) have received recent attention.[1−4] The advantages of such "all-carbon" (or more accurately, "mostly carbon") active layers include low cost, solution processing, air stability, high thermal resistance, excellent light absorption, and widely tunable electronic properties.[3,5] For example, controlling the relative amounts of sp^2 and sp^3 hybridization[6] in a-C enables broad tunability of the optical properties, leading to sunlight absorption efficiencies comparable to amorphous silicon.[1]

Solar cells based on carbon nanomaterials have been explored both computationally and experimentally, with results showing broad spectral absorption and high carrier mobility as well as thermal, chemical, and optical stability.[2−4,7,8] In general, in these devices the all-carbon photoactive layer consists of semiconducting single-walled carbon nanotubes (SWCNTs) as light-absorbing component and charge-donating (donor) material interfaced with fullerene derivatives as charge-accepting (acceptor) material.[2−4,7,9] Such cells generally have a power conversion efficiency (PCE) <1% for near-infrared illumination, but accurate geometry optimization has led to a record-high efficiency of 3.1%.[10] However, SWCNTs are typically mixtures of different tubes with various chiralities and nonhomogeneous diameters, making control over the bandgap difficult, thus reducing device performance and limiting scalability. This scenario motivates the search for bulk carbon materials possessing the same desirable features of carbon nanomaterials coupled to large-scale manufacturability and low cost. In this respect, amorphous carbon (a-C) represents an appealing candidate because it can be routinely deposited in thin-film form with accurate control of its structural and chemical properties. Indeed, although application of a-C in solar cells has been very limited thus far, the structure, bonding, stoichiometry, and hydrogen content of a-C have been correlated with properties linked to PV performance.[1]

Here we report a computational study of a-C to be employed as active PV layer in bulk heterojunctions (BHJs). Of particular relevance is whether a-C-based materials would enable successful electron or hole extraction as well as reduced sources of carrier recombination, possibly substituting the electron acceptor or donor in all-C BHJs. We carry out ab initio molecular dynamics (MD) and density functional theory (DFT) calculations for a large statistical set of interfaces between a-C at different densities and two types of carbon nanostructures (semiconducting SWCNT with (10,0) chirality and fullerene C_{60}) with the aim of relating the optoelectronic and PV properties of the interfaces to the density and structure of a-C. We also considered a-C doping to further engineer the heterostructure. In particular, we incorporated nitrogen (n-type) and boron (p-type) atoms in a-C samples. Here we

Received: February 26, 2017
Accepted: March 16, 2017
Published: March 16, 2017

DOI: 10.1021/acsenergylett.7b00166
ACS Energy Lett. 2017, 2, 882−888

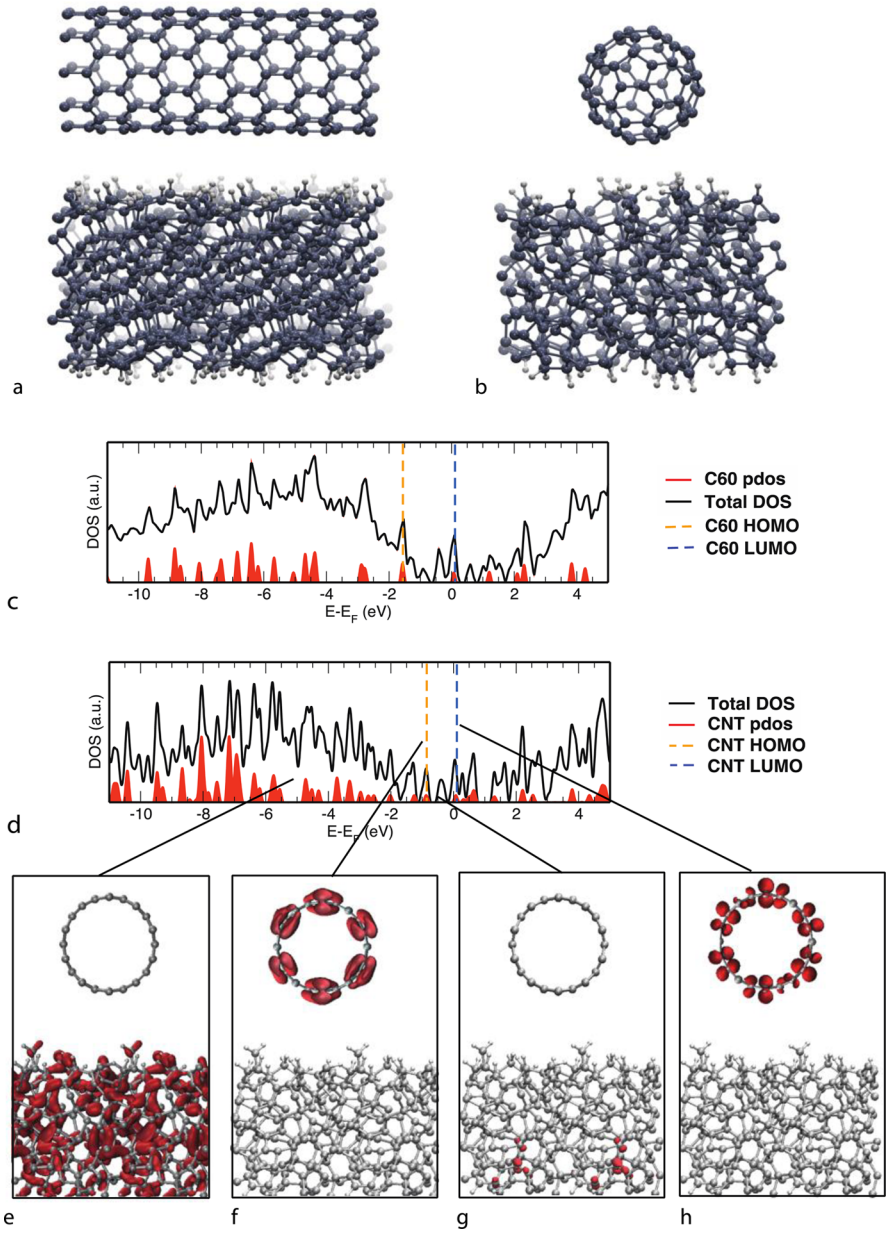

Figure 1. Interface calculation results for a-C at $\rho \approx 3.00$ g/cm^3: (a) Ball-and-stick representation of the interface CNT/a-C. (b) Ball-and-stick representation of the interface C_{60}/a-C. (c) DOS and PDOS of C_{60}/a-C interface. (d) DOS and PDOS of SWCNT/a-C interface. Electronic density isosurfaces of the SWCNT/a-C interface states at different energies. An example of a delocalized state in the valence band (e), of the SWCNT HOMO state (f), of a semilocalized state (g), and of the SWCNT LUMO state (h) is represented.

consider only a-C because the hydrogenation has only a minor effect on optoelectronic properties.[1] Using DFT, the structural features such as the density and fraction of sp^2- and sp^3-hybridized C atoms are correlated with the electronic structure and photon absorption of the interface structures.

Our results show that the energy alignment between the a-C mobility edges and the occupied and unoccupied states of the SWCNT or C_{60} can be selected by varying the a-C density and doping to obtain a type-II interface. This is a crucial prerequisite to separate electron/hole charges and generate a photocurrent given the large exciton binding typical of these materials. Taken together, our results suggest that a-C represents a promising active layer component for carbon-based solar cells.

The amorphous bulk structures were prepared using a multistep protocol: The atomic positions were initially randomized using the algorithm from Wooten, Winer, and Weaire;[11] once randomized, the a-C samples were annealed at 5000 K (above the diamond and graphite melting temperatures[12]) for 3 ps using first-principles MD and subsequently cooled to 300 K over 0.3 ps and then further equilibrated for 3 ps.[13] First-principles MD calculations were based on DFT, as implemented in the Vienna Ab-initio Simulation Package (VASP).[14] In brief, the Kohn−Sham Hamiltonian of the system included projector-augmented wave pseudopotentials to describe the core−valence electron interaction[15,16] and the local density approximation (LDA) of the exchange-correlation potential.[17] The Kohn−Sham wave functions were expanded in plane waves with a kinetic energy cutoff of 350 eV, the Brillouin

DOI: 10.1021/acsenergylett.7b00166
ACS Energy Lett. 2017, 2, 882−888

zone was sampled at the Γ point, and the NVT ensemble was adopted in MD simulations. The high annealing temperature and the fast quench rate were here utilized for computational efficiency. Trends in the resulting structures are in good agreement with previous computational and experimental work.[1,18,19] All final structures were relaxed within DFT to $<10^{-4}$ eV/Å in the residual atomic forces. The a-C bulk structures are generated in cubic supercells containing 216 C atoms for a range of densities from 2.0 to 3.5 g/cm^3 with increments of 0.25 g/cm^3 for a total of seven different densities. Each simulation cell has a variable dimension ranging between 12.91 and 10.71 Å.[20] Doped a-C structures were obtained by randomly removing one, two, or three C atoms from the supercell and replacing them with atoms of a different element (nitrogen or boron); this is equivalent to dopant concentrations of 0.46, 0.93, and 1.38%.[21−23]

Surface structures of amorphous carbon were obtained by cleaving from the bulk structure slabs of 10 Å thickness and hydrogenating the two generated surfaces to saturate dangling bonds. Calculations were performed in orthorhombic supercells containing the a-C slab and a vacuum region >15 Å to avoid spurious interactions between periodic replicas. Subsequently these slabs were used to build interfaces both with fullerene and with a (10,0) SWCNT, which can be considered prototypical test cases of semiconductor−semiconductor junctions between C-based nanostructures and a-C. The Brillouin zone for these interface systems was sampled employing a 2 × 1 × 1 Monkhorst−Pack[24] mesh to account for the SWCNT periodicity. To obtain meaningful statistical averages of the electronic properties of the interfaces, we prepared 10 samples for each a-C density (both with fullerene and SWCNT) and dopant species/concentration.

Electronic and optical properties reported were obtained using LDA, although we also verified for some of the final structures that employing the HSE06 hybrid exchange functional[25,26] does not qualitatively alter the trends obtained using LDA (in particular, the level alignments of the heterostructures). Optical absorption spectra were computed within the independent-particle approximation using the Kohn−Sham eigenvalues and wave functions and including up to 1000 empty bands. Convergence with respect to all computed properties was carefully verified.

The structural properties of the a-C slabs used to represent a-C surfaces were analyzed in terms of the radial distribution function, carbon coordination number, and sp^3/sp^2 ratio. Our analysis indicates that the fraction of sp^3-, sp^2-, and sp-hybridized C atoms depends strongly on the density of the sample. In agreement with previous work,[1] the sp^3 fraction increases from 10 to 90% as the density increases toward that of diamond, while the fraction of sp^2 atoms decreases from 80 to 10% over the same interval. The sp fraction is minimal, and appreciable values of 5−10% are present only at densities close to that of graphite. Our observation of sp^3 hybridization at increasing densities is consistent with experimental studies of a-C.[18,19,27,28] We observe a tendency of sp^3 C atoms to form distorted tetrahedra arranged in a 3-D network, while sp^2 C atoms preferentially arrange in planar clusters such as chain or ring units with fewer than 10 C atoms. At higher densities close to that of diamond, the structures present fewer dangling bonds. At lower densities close to that of graphite, the corresponding structures show a larger fraction of dangling bonds.

Interfaces containing a-C slabs are formed by placing a C_{60} or a (10,0) CNT at a distance of 4 Å from the a-C surfaces and fully relaxing the system. Typical configurations of C_{60} and SWCNT on a-C are represented in Figure 1a,b. Calculations show that C_{60} and SWCNT adsorb at all considered surfaces, reducing the distance between a-C and the nanostructure to ∼3 Å, slightly less than the equilibrium graphene/graphene distance calculated with LDA, with average binding energies[29] of 0.80 ± 0.07 and 0.95 ± 0.04 eV per cell for the SWCNT- and C_{60}-based systems, respectively.

To provide insight into the electronic properties of these interface systems, the density of states (DOS) and projected DOS (PDOS) were calculated and averaged over the 10 samples for each a-C density (Supporting Information Figures S2 and S3). For a-C samples with higher densities ($\rho \geq 3.00$ g/cm^3), we predict a band gap of ∼4 eV, close to the LDA-calculated gap of diamond (4.1 eV[30]). For a-C samples characterized by lower ρ, an increasing number of states associated with sp^2 hybridization appears within the gap established by the sp^3 framework. Analysis of the PDOS shows that the valence band maximum and conduction band minimum values for $\rho \leq 2.75$ to 3.00 g/cm^3 are contributed mostly by p states of the sp^2 C atoms, while s and p states of sp^3 C atoms are found at energies lower (higher) than the valence (conduction) band maximum (minimum). In particular, at densities <3.00 g/cm^3, we observe the formation of extended π states contributed by p states from the sp^2 C atoms that give rise to closure of the gap as the sp^2 fraction increases for structures with lower densities.

In the a-C/SWCNT systems, the SWCNT lowest unoccupied molecular orbital (LUMO) is located within the a-C energy gap, slightly above the Fermi energy (E_F), whereas the highest occupied molecular orbital (HOMO) falls ∼1 eV below E_F (See Figure 1d). The average energy gap ($\Delta E^{\mathrm{LUMO-HOMO}}$) of the SWCNT is 0.87 ± 0.02 eV, larger than that of the isolated (10,0) SWCNT calculated at the same level of theory ($\Delta E_{\mathrm{isolated}}{}^{\mathrm{LUMO-HOMO}} = 0.82$ eV). Similarly, for the C_{60}/a-C systems the C_{60} LUMO states lie immediately above E_F, while the C_{60} HOMO appears 1 eV below E_F (See Figure 1c). In these systems, the average C_{60} $\Delta E^{\mathrm{LUMO-HOMO}}$ is 1.33 ± 0.01 eV, again slightly larger than the isolated C_{60} gap (1.27 eV).

Figure 1e−h represents the charge density isosurfaces associated with KS states of different energies for the SWCNT/a-C interface for $\rho \approx 3.00$ g/cm^3. We observe that the localization of the orbitals originating from a-C strongly correlates with the energy position of KS states with respect to E_F. States with energy near E_F are typically spatially localized over a few C atoms and associated with the presence of unpassivated bonds within the amorphous network. Moving into the valence (conduction) band, we observe progressively more delocalized states. Such states of semidelocalization (Figure 1g) are associated with disorder or strain due to bond and angle distortion. States extending over the entire a-C region originate from energy levels deep inside the valence and conduction bands (Figure 1e). The frontier orbitals of both SWCNT and C_{60} do not present any hybridization with the a-C substrate when interfaced with a-C (see Figure 1f−h). To determine the level alignment when an amorphous phase is involved in a heterostructure, it is crucial to recognize the states that mark the transition between localized and delocalized states in a-C because the latter states contribute efficiently to charge transport. These energies are referred to as the valence

DOI: 10.1021/acsenergylett.7b00166
ACS Energy Lett. 2017, 2, 882−888

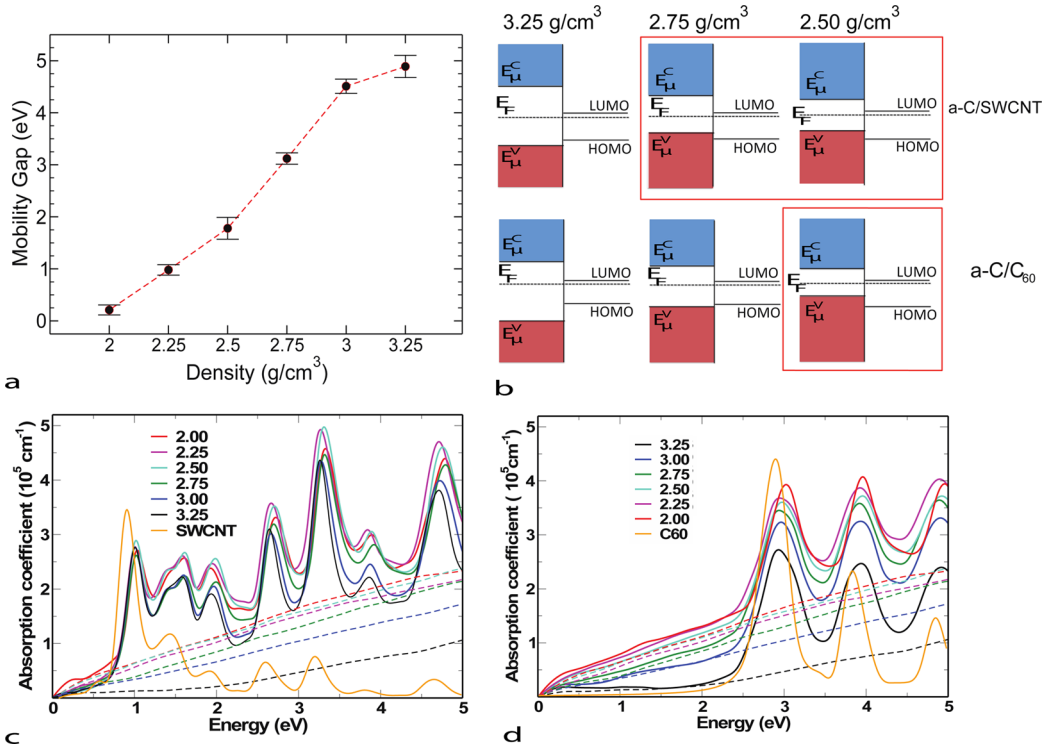

Figure 2. (a) Average mobility gaps as a function of a-C density in SWCNT/a-C interfaces. (b) Schematic energy level alignments between a-C mobility edges and fullerene HOMO and LUMO states in a-C/SWCNT and a-C/C_{60} interfaces. The positions of energy levels are calculated with an uncertainty <0.07 eV. Absorption coefficient in the solar photon energy range, shown as a function of a-C density in SWCNT/a-C (c) and C_{60}/a-C (d) interfaces represented with continuous lines and absorption coefficient for isolated a-C slabs as a function of a-C density reported with dashed lines.

and conduction band mobility edges $E_{V\mu}$ and $E_{C\mu}$, respectively, and their difference is the mobility gap, $E_\mu = E_{C\mu} - E_{V\mu}$, which can be considered similar to the energy gap in crystalline semiconductors. We compute the localization of KS states by employing the method based on calculating the inverse participation ratios (IPRs) and following the procedure reported in ref 31. In this specific case, IPR is defined as IPR = $1/(\sum_i 1/c_i)$ where the c_i coefficients correspond to atomic contributions to the wave function of the -*i*th state, taking into account only the C-atom contributions belonging to a-C slabs. The IPR analysis shows sharp transitions for decreasing (increasing) energies in the valence (conduction) band, allowing us to identify the mobility edges and thus the mobility gaps. (See Supporting Informaiton Figure S4 for further details.)

The average mobility gap as a function of the a-C density is shown in Figure 2a for the SWCNT/a-C interfaces (mobility gaps for C_{60}/a-C systems assume similar values to within 1%). The calculated E_μ values fall in the range 0−5 eV and decrease monotonically as ρ moves from diamond to graphite densities. This trend is associated with an increasing overlap between π or π^* states originating from C atoms belonging to the a-C slabs, in agreement with E_μ calculated previously for bulk a-C structures using the HSE06 functional.[1] As demonstrated in ref 1, this variability highlights the possibility of tailoring the electronic properties of the interfaces by controlling the density of the sample. This result is in sharp contrast with amorphous silicon, for which E_μ can be tuned only by a fraction of an electronvolt (<0.08 eV).[32]

To allow efficient harvesting of solar energy in a BHJ cell, it is essential that charge separation occurs at the interface between the SWCNT or C_{60} and a-C when an exciton is formed: This requires a type-II (staggered) heterostructure. In particular, for the systems studied here, $E_{C\mu}$ has to be sufficiently high in energy for efficient electron injection in the unoccupied fullerene states, while $E_{V\mu}$ should be positioned inside the fullerene or SWCNT band gap to avoid direct electron/hole recombination. In Figure 2b, we show the energy level alignments between a-C mobility edges and the fullerene (or SWCNT) HOMO and LUMO. It is apparent that the a-C $E_{V\mu}$ lies in the SWCNT (C_{60}) energy gap only for samples with density <3.00 g/cm^3 (2.75 g/cm^3), while $E_{C\mu}$ always lies at energies higher than the LUMO both for the SWCNT and C_{60}. A type-II alignment is achieved at the SWCNT/a-C and C_{60}/a-C interfaces only for a specific a-C density range, where a-C behaves as the donor and the fullerene or nanotube as the acceptor. To overcome the problems possibly arising from the presence of trap states between the a-C mobility edges and thus improve cell performances, we suggest to employ a-C active layers characterized by a thickness of the order of magnitude of the electron/hole diffusion length.

Figure 2c,d shows our calculated optical absorption coefficient α (units of cm^{-1}) for a-C/C_{60} and a-C/SWCNT interfaces with different a-C densities. At all densities, we observe relatively large absorbance values (>10^5 cm^{-1}) at visible photon energies, which are comparable to the absorption in the best organic and inorganic absorbers employed in PV.[33−35] This feature also makes a-C-based interfaces excellent candidate materials for sunlight harvesting in BHJ devices. In particular, we observe that absorption in the visible energy range is mainly determined by interband transitions between π and π^* states of the a-C, consistently with the electronic structure analysis

DOI: 10.1021/acsenergylett.7b00166
ACS Energy Lett. 2017, 2, 882−888

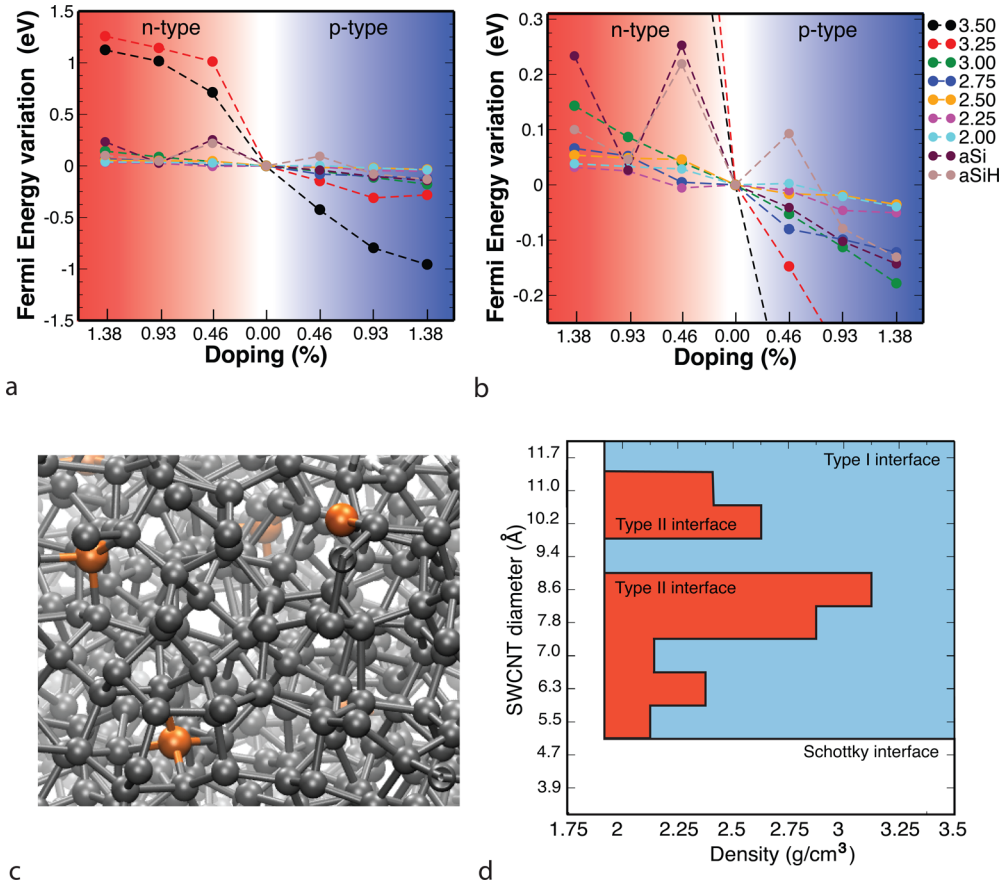

Figure 3. (a) Average Fermi energy variation with respect dopant concentration. (b) Zoom in the energy (*y* axis) of panel a. (c) Ball-and-stick representation of an example of a doped a-C structure for a density of 3.25 g/cm^3. (d) Interface type diagram of a-C/SWCNT interface reported as a function of a-C density and diameter of SWCNT of chirality (*n*,0) with *n* = 5, 6, 7, ..., 15.

presented above. SWCNT- and C_{60}-based interfaces with low a-C density present a large fraction of sp^2 C atoms and consequently show large absorption values due to the presence of extended π states. In contrast, samples with a-C densities >3.00 g/cm^3 and lower π conjugation show absorption onsets at higher energies and can absorb sunlight significantly only at energies larger than 2.5 to 3 eV. These trends suggest that low-density a-C-based structures, favoring extended π conjugation and forming type-II interfaces, are best for PV applications. Optical absorption in these interfaces shows a slight blue shift of the peaks associated with the SWCNT and C_{60}, in agreement with the electronic structure calculations and an overall increase in absorption intensity compared with isolated a-C absorption for samples with the same density due to the interaction between SWCNT and C_{60} and a-C slabs. The blue shift is higher in samples with lower densities.

Having shown the applicability of a-C in all carbon-based PV cells, we now propose further optimization of these cells by engineering one of the components of the BHJ. We first consider doping of the a-C component; then, we study the effect of changing the blended nanostructure (namely, controlling the NT chirality).

Introduction of dopants (such as N and B impurities) in intrinsic a-C substrates strongly affects optoelectronic properties, as shown by our analysis of the structural and electronic properties (including DOS, PDOS, and mobility gap) of a range of doped samples. (See Supporting Information for details.) We found that the p-type (n-type) dopants add one or more unoccupied (occupied) states in the forbidden energy gap right above the valence band maximum (below the conduction band minimum), as reported in Figures S5 and S6, without modifying the mobility gap of the undoped a-C material (Figure S7), and the Fermi level lies close to the impurity levels.

Figure 3a,b reports the dependence of the Fermi level[36] position as a function of the nominal n- and p- doping for a-C samples at different densities. Pure (a-Si) and hydrogenated (a-Si:H) are reported for the sake of comparison calculated using the same approach.[37] At all densities, we observe a relatively large Fermi level shift as a function of the dopant chemistry. The effect in a-C is larger than that observed for doped a-Si and a-Si:H. In particular, the DFT results show a progressive reduction (increase) in energy of the Fermi level moving from values higher (lower) than 1 eV (−1 eV) with respect to the Fermi level position of the undoped samples when the n-type (p-type) dopant content decreases from 1.38 to 0%. A strong dependence on the a-C density is observed as well, with an increase of >1 eV as the density changes from that of graphite to more diamond-like. This means that when a-C materials and C-based nanostructures (such as SWCNT and C_{60}) are brought in contact, the Fermi levels align, giving rise to different band offsets. Therefore, besides the advantages of doped a-C such as more efficient charge transport and enhanced carrier mobility, it is possible to tune the band offsets controlling the doping concentration so as to design BHJ interfaces where the a-C material may act either as donor or as acceptor. Such doped a-C

DOI: 10.1021/acsenergylett.7b00166
ACS Energy Lett. 2017, 2, 882−888

films could also, in principle, be employed to realize a p−n junction, although this aspect of such materials will be the subject of future work.

A different way to tune the heterostructure and its energy alignment is to modify the acceptor phase. The bandgap of both fullerenes and SWCNTs is dependent on their size.[38] Figure 3d shows an example of how this tunability can be utilized in these interfaces. Here we plot the interface type versus SWCNT diameter (data for zigzag (n,0) nanotube bandgaps are taken from ref 38). In this specific case, a Schottky interface (white area in Figure 3d) is obtained either if the SWCNT diameter (d_{SWCNT}) is <5 Å or if a-C has a density <2.00 g/cm^3. Type-I alignment (blue area) is typical of interfaces with high-density a-C or for SWCNT with band gap <0.05 eV (for example, with (12,0) and (15,0) CNTs). Finally, DFT results show that for specific chiralities, interfaces of type II (red area) can be realized with a-C ρ of ∼3.00 g/cm^3.

In conclusion, we established that the energy alignment between the a-C mobility edges and the occupied and unoccupied states of the SWCNT or C_{60} can be widely tuned by varying the a-C density, the dopant content, and the nanostructure size to realize type-II interfaces. The employment of a-C films with lower density is to be preferred for undoped nanostructures. Our results suggest that a-C-based interfaces exhibit excellent sunlight absorption, in particular, interfaces with a-C ρ <2.75 g/cm^3. In addition, we demonstrated that the heterostructures and their energy alignment can be further tuned, introducing dopants in a-C or changing the acceptor phase (as, for example, modifying SWCNT diameter). Doping also allows modulating the conductivity of the film, thus overcoming charge-transport issues typical of amorphous phases.

Taken together, our results demonstrate that a-C can be employed as an active layer material in PV. The successful preparation of a BHJ device based on a-C would require additional optimization steps, including a suitable device architecture with a-C active layer thickness of about the electron/hole diffusion length so as to reduce the carrier recombination that, as known, is one of the main issues in an amorphous structure.[39,40] The new insights presented here may open up new opportunities for the optimization of a-C in this challenging area.

■ ASSOCIATED CONTENT

Supporting Information

The Supporting Information is available free of charge on the ACS Publications website at DOI: 10.1021/acsenergylett.7b00166.

Average radial distribution functions, average density of states of a-C/SWCT interfaces with respect to a-C density, average density of states of a-C/C_{60} interfaces with respect to a-C density, inverse participation ratio, nitrogen and boron doping in a-C, density of states, and average mobility gap. (PDF)

■ AUTHOR INFORMATION

Corresponding Author

*Tel: 617-324-3566. E-mail: jcg@mit.edu.

ORCID

Francesca Risplendi: 0000-0002-1277-6733

Notes

The authors declare no competing financial interest.

■ ACKNOWLEDGMENTS

We thank NERSC and XSEDE for providing computational resources. This work was partially supported by the Eni Solar Frontiers Program at MIT.

■ REFERENCES

(1) Risplendi, F.; Bernardi, M.; Cicero, G.; Grossman, J. C. Structure-Property Relations in Amorphous Carbon for Photovoltaics. *Appl. Phys. Lett.* **2014**, *105*, 043903−043907.

(2) Jain, R. M.; Howden, R.; Tvrdy, K.; Shimizu, S.; Hilmer, A. J.; McNicholas, T. P.; Gleason, K. K.; Strano, M. S. Polymer-Free Near-Infrared Photovoltaics with Single Chirality (6,5) Semiconducting Carbon Nanotube Active Layers. *Adv. Mater.* **2012**, *24*, 4436−4439.

(3) Bernardi, M.; Lohrman, J.; Kumar, P. V.; Kirkeminde, A.; Ferralis, N.; Grossman, J. C.; Ren, S. Nanocarbon-Based Photovoltaics. *ACS Nano* **2012**, *6*, 8896−8903.

(4) Tung, V. C.; Huang, J.-H.; Tevis, I.; Kim, F.; Kim, J.; Chu, C.-W.; Stupp, S. I.; Huang, J. Surfactant-Free Water-Processable Photoconductive All-Carbon Composite. *J. Am. Chem. Soc.* **2011**, *133*, 4940−4947.

(5) Zhu, H.; Wei, J.; Wang, K.; Wu, D. Applications of Carbon Materials in Photovoltaic Solar Cells. *Sol. Energy Mater. Sol. Cells* **2009**, *93*, 1461−1470.

(6) Robertson, J. Amorphous Carbon. *Adv. Phys.* **1986**, *35*, 317−374.

(7) Bindl, D. J.; Wu, M.-Y.; Prehn, F. C.; Arnold, M. S. Efficiently Harvesting Excitons from Electronic Type-Controlled Semiconducting Carbon Nanotube Films. *Nano Lett.* **2011**, *11*, 455−460.

(8) Tune, D. D.; Shapter, J. G. The Potential Sunlight Harvesting Efficiency of Carbon Nanotube Solar Cells. *Energy Environ. Sci.* **2013**, *6*, 2572−2577.

(9) Wang, H.; Koleilat, G. I.; Liu, P.; Jiménez-Osès, G.; Lai, Y.-C.; Vosgueritchian, M.; Fang, Y.; Park, S.; Houk, K. H.; Bao, Z. High-Yield Sorting of Small-Diameter Carbon Nanotubes for Solar Cells and Transistors. *ACS Nano* **2014**, *8* (3), 2609−2617.

(10) Gong, M.; Shastry, T. A.; Xie, Y.; Bernardi, M.; Jasion, D.; Luck, K. A.; Marks, T. B.; Grossman, J. C.; Ren, S.; Hersam, M. C. Polychiral Semiconducting Carbon Nanotube−Fullerene Solar Cells. *Nano Lett.* **2014**, *14*, 5308−5314.

(11) Wooten, F.; Winer, K.; Weaire, D. Computer Generation of Structural Models of Amorphous Si and Ge. *Phys. Rev. Lett.* **1985**, *54*, 1392−1397.

(12) *CRC Handbook of Chemistry and Physics*, 92nd ed.; Haynes, W. M., Ed.; CRC Press, 2011; 4.121−4.123.

(13) We have verified that our cooling rate was sufficiently slow by comparing the results with those obtained with simulations with 10× slower cooling rates. No substantial differences in structural and electronic properties have been found with lower annealing temperatures of 4500 and 4800 K. Before performing electronic structure calculations, all structures were relaxed within DFT to <10^{-4} eV/Å in the residual atomic forces.

(14) Kresse, G.; Furthmüller, J. Efficient iterative schemes for *ab initio* total-energy calculations using a plane-wave basis set. *Phys. Rev. B: Condens. Matter Mater. Phys.* **1996**, *54*, 11169−11186.

(15) Blöchl, P. E. Projector augmented-wave method. *Phys. Rev. B: Condens. Matter Mater. Phys.* **1994**, *50*, 17953−17979.

(16) Kresse, G.; Joubert, D. From ultrasoft pseudopotentials to the projector augmented-wave method. *Phys. Rev. B: Condens. Matter Mater. Phys.* **1999**, *59*, 1758−1775.

(17) Perdew, J. P.; Zunger, A. Self-interaction correction to density-functional approximations for many-electron systems. *Phys. Rev. B: Condens. Matter Mater. Phys.* **1981**, *23*, 5048−5079.

(18) Weiler, M.; Sattel, S.; Giessen, T.; Jung, K.; Ehrhardt, H.; Veerasamy, V. S.; Robertson, J. Preparation and properties of highly tetrahedral hydrogenated amorphous carbon. *Phys. Rev. B: Condens. Matter Mater. Phys.* **1996**, *53*, 1594−1608.

(19) Fallon, P. J.; Veerasamy, V. S.; Davis, C. A.; Robertson, J.; Amaratunga, G. A.; Milne, W. I.; Koskinen, J. Properties of filtered-ion-

DOI: 10.1021/acsenergylett.7b00166
ACS Energy Lett. 2017, 2, 882−888

beam-deposited diamondlike carbon as a function of ion energy. *Phys. Rev. B: Condens. Matter Mater. Phys.* **1994**, *49*, 2287−2293.
(20) Orthorhombic supercells are employed to take into account the SWCNT periodicity. The surface lattice parameter a is fixed to a multiple of SWCNT periodicity (4.233 Å) and b corresponds to twice the SWCNT diameter. The number of C atoms included in a-C slabs varies between 188 and 256 depending on the sample density.
(21) Sitch, P. K.; Kohler, Th.; Jungnickel, G.; Porezag, D.; Frauenheim, Th. A theoretical study of boron and nitrogen doping in tetrahedral amorphous carbon. *Solid State Commun.* **1996**, *100* (8), 549−553.
(22) Zheng, B.; Zheng, W. T.; Zhang, W.; Wen, Q. B.; Zhu, J. Q.; Meng, S. H.; He, X. D.; Han, J. C. First-Principle Study of Nitrogen Incorporation in Amorphous Carbon. *Carbon* **2006**, *44*, 962−968.
(23) Miyajima, Y.; Tison, Y.; Giusca, C. E.; Stolojan, V.; Watanabe, H.; Habuchi, H.; Henley, S. J.; Shannon, J. M.; Silva, S. R. P. Probing the band structure of hydrogen-free amorphous carbon and the effect of nitrogen incorporation. *Carbon* **2011**, *49* (15), 5229−5238.
(24) Monkhorst, H. J.; Pack, J. D. Special points for Brillouin-zone integrations. *Phys. Rev. B* **1976**, *13*, 5188−5192.
(25) Paier, J.; Marsman, M.; Hummer, K.; Kresse, G.; Gerber, I. C.; Angyan, J. G. Screened hybrid density functionals applied to solids. *J. Chem. Phys.* **2006**, *124*, 154709−154713.
(26) Paier, J.; Marsman, M.; Hummer, K.; Kresse, G.; Gerber, I. C.; Angyan, J. G. Erratum: "Screened hybrid density functionals applied to solids" [J. Chem. Phys. 124, 154709 (2006)]. *J. Chem. Phys.* **2006**, *125*, 249901−249901.
(27) Ferrari, A. C.; Libassi, A.; Tanner, B. K.; Stolojan, V.; Yuan, J.; Brown, L. M.; Rodil, S. E.; Kleinsorge, B.; Robertson, J. Density, sp3 fraction, and cross-sectional structure of amorphous carbon films determined by x-ray reflectivity and electron energy-loss spectroscopy. *Phys. Rev. B: Condens. Matter Mater. Phys.* **2000**, *62*, 11089−11103.
(28) Fallon, P. J.; Veerasamy, V. S.; Davis, C. A.; Robertson, J.; Amaratunga, G. A.; Milne, W. I.; Koskinen, J. Properties of filtered-ion-beam-deposited diamondlike carbon as a function of ion energy. *Phys. Rev. B: Condens. Matter Mater. Phys.* **1993**, *48*, 4777−4782.
(29) The binding energy (BE) of the C nanostructure to the a-C surfaces was evaluated by calculating BE = $E^{tot} - E^{surf} - E^{C\text{-}struct}$, where E^{tot} is the total energy for absorbed system and E^{surf} and $E^{C\text{-}struct}$ correspond to total energy of the relaxed clean surface and isolated SWCNT or C_{60}, respectively.
(30) Surh, M. P.; Louie, S. G.; Cohen, M. L. Band gaps of diamond under anisotropic stress. *Phys. Rev. B: Condens. Matter Mater. Phys.* **1992**, *45*, 8239−8247.
(31) Baskaran, N.; Ghule, A.; Bhongale, C.; Murugan, R.; Chang, H. Phase transformation studies of ceramic $BaTiO_3$ using thermo-Raman and dielectric constant measurements. *J. Appl. Phys.* **2002**, *91*, 10038−10043.
(32) Legesse, M.; Nolan, M.; Fagas, G. Revisiting the Dependence of the Optical and Mobility Gaps of Hydrogenated Amorphous Silicon on Hydrogen Concentration. *J. Phys. Chem. C* **2013**, *117* (45), 23956−23963.
(33) Xing, G.; Mathews, N.; Sun, S.; Lim, S. S.; Lam, Y. M.; Grätzel, M.; Mhaisalkar, S.; Sum, T. C. Long-Range Balanced Electron- and Hole-Transport Lengths in Organic-Inorganic $CH_3NH_3PbI_3$. *Science* **2013**, *342*, 344−347.
(34) Green, M. A.; Keevers, M. J. Short Communication: Optical Properties of Intrinsic Silicon at 300 K. *Prog. Photovoltaics* **1995**, *3* (3), 189−192.
(35) Hwang, J.; Schwendeman, I.; Ihas, B. C.; Clark, R. J.; Cornick, M.; Nikolou, M.; Argun, A.; Reynolds, J. R.; Tanner, D. B. In situ measurements of the optical absorption of dioxythiophene-based conjugated polymers. *Phys. Rev. B: Condens. Matter Mater. Phys.* **2011**, *83*, 195121−195133.
(36) Fermi energy difference is evaluated for bulk samples with the same supercell.
(37) We used cubic simulation cells containing 216 Si atoms for the a-Si samples and introduced 20% H atoms in the case of a-Si:H. The amorphous structures were prepared using the same multistep MD protocol employed for a-C and a-C:H. The optoelectronic properties of the final systems were averaged over 10 samples.
(38) Sharma, U. S.; Srivastava, A.; Verma, U. P. Ab-Initio Study of Zigzag Single Wall Carbon Nanotubes. *J. Comput. Theor. Nanosci.* **2010**, *7* (8), 1479−1481.
(39) Heitz, T.; Godet, C.; Bourèe, J. E.; Drèvillon, B.; Conde, J. P. Radiative and nonradiative recombination in polymerlike a-C:H films. *Phys. Rev. B: Condens. Matter Mater. Phys.* **1999**, *60*, 6045−6052.
(40) Robertson, J. *Mater. Sci. Eng., R* **2002**, *37*, 129−281.

DOI: 10.1021/acsenergylett.7b00166
ACS Energy Lett. 2017, 2, 882−888